CLEO CONF95-6
EPS0160
July 7, 1995

Update on Exclusive $B^0 \to K^{*0}(892)\gamma$ Measurement at CLEO

K.W. Edwards,[1] K.W. McLean,[1] M. Ogg,[1] A. Bellerive,[2] D.I. Britton,[2] E.R.F. Hyatt,[2] R. Janicek,[2] D.B. MacFarlane,[2] P.M. Patel,[2] B. Spaan,[2] A.J. Sadoff,[3] R. Ammar,[4] P. Baringer,[4] A. Bean,[4] D. Besson,[4] D. Coppage,[4] N. Copty,[4] R. Davis,[4] N. Hancock,[4] S. Kotov,[4] I. Kravchenko,[4] N. Kwak,[4] Y. Kubota,[5] M. Lattery,[5] M. Momayezi,[5] J.K. Nelson,[5] S. Patton,[5] R. Poling,[5] V. Savinov,[5] S. Schrenk,[5] R. Wang,[5] M.S. Alam,[6] I.J. Kim,[6] Z. Ling,[6] A.H. Mahmood,[6] J.J. O'Neill,[6] H. Severini,[6] C.R. Sun,[6] F. Wappler,[6] G. Crawford,[7] R. Fulton,[7] D. Fujino,[7] K.K. Gan,[7] K. Honscheid,[7] H. Kagan,[7] R. Kass,[7] J. Lee,[7] M. Sung,[7] C. White,[7] A. Wolf,[7] M.M. Zoeller,[7] X. Fu,[8] B. Nemati,[8] W.R. Ross,[8] P. Skubic,[8] M. Wood,[8] M. Bishai,[9] J. Fast,[9] E. Gerndt,[9] J.W. Hinson,[9] T. Miao,[9] D.H. Miller,[9] M. Modesitt,[9] E.I. Shibata,[9] I.P.J. Shipsey,[9] P.N. Wang,[9] L. Gibbons,[10] S.D. Johnson,[10] Y. Kwon,[10] S. Roberts,[10] E.H. Thorndike,[10] T.E. Coan,[11] J. Dominick,[11] V. Fadeyev,[11] I. Korolkov,[11] M. Lambrecht,[11] S. Sanghera,[11] V. Shelkov,[11] T. Skwarnicki,[11] R. Stroynowski,[11] I. Volobouev,[11] G. Wei,[11] M. Artuso,[12] M. Gao,[12] M. Goldberg,[12] D. He,[12] N. Horwitz,[12] S. Kopp,[12] G.C. Moneti,[12] R. Mountain,[12] F. Muheim,[12] Y. Mukhin,[12] S. Playfer,[12] S. Stone,[12] X. Xing,[12] J. Bartelt,[13] S.E. Csorna,[13] V. Jain,[13] S. Marka,[13] D. Gibaut,[14] K. Kinoshita,[14] P. Pomianowski,[14] B. Barish,[15] M. Chadha,[15] S. Chan,[15] D.F. Cowen,[15] G. Eigen,[15] J.S. Miller,[15] C. O'Grady,[15] J. Urheim,[15] A.J. Weinstein,[15] F. Würthwein,[15] D.M. Asner,[16] M. Athanas,[16] D.W. Bliss,[16] W.S. Brower,[16] G. Masek,[16] H.P. Paar,[16] J. Gronberg,[17] C.M. Korte,[17] R. Kutschke,[17] S. Menary,[17] R.J. Morrison,[17] S. Nakanishi,[17] H.N. Nelson,[17] T.K. Nelson,[17] C. Qiao,[17] J.D. Richman,[17] D. Roberts,[17] A. Ryd,[17] H. Tajima,[17] M.S. Witherell,[17] R. Balest,[18] K. Cho,[18] W.T. Ford,[18] M. Lohner,[18] H. Park,[18] P. Rankin,[18] J.G. Smith,[18] J.P. Alexander,[19] C. Bebek,[19] B.E. Berger,[19] K. Berkelman,[19] K. Bloom,[19] T.E. Browder,[19*] D.G. Cassel,[19] H.A. Cho,[19] D.M. Coffman,[19] D.S. Crowcroft,[19] M. Dickson,[19] P.S. Drell,[19] D.J. Dumas,[19] R. Ehrlich,[19] R. Elia,[19] P. Gaidarev,[19] M. Garcia-Sciveres,[19] B. Gittelman,[19] S.W. Gray,[19] D.L. Hartill,[19] B.K. Heltsley,[19] S. Henderson,[19] C.D. Jones,[19] S.L. Jones,[19] J. Kandaswamy,[19] N. Katayama,[19] P.C. Kim,[19] D.L. Kreinick,[19] T. Lee,[19] Y. Liu,[19] G.S. Ludwig,[19] J. Masui,[19] J. Mevissen,[19] N.B. Mistry,[19] C.R. Ng,[19] E. Nordberg,[19] J.R. Patterson,[19] D. Peterson,[19] D. Riley,[19] A. Soffer,[19] P. Avery,[20] A. Freyberger,[20] K. Lingel,[20] C. Prescott,[20] J. Rodriguez,[20] S. Yang,[20] J. Yelton,[20] G. Brandenburg,[21] D. Cinabro,[21] T. Liu,[21] M. Saulnier,[21] R. Wilson,[21] H. Yamamoto,[21] T. Bergfeld,[22] B.I. Eisenstein,[22] J. Ernst,[22] G.E. Gladding,[22] G.D. Gollin,[22] M. Palmer,[22] M. Selen,[22] and J.J. Thaler[22]

(CLEO Collaboration)

[1]*Carleton University, Ottawa, Ontario K1S 5B6 and the Institute of Particle Physics, Canada*
[2]*McGill University, Montréal, Québec H3A 2T8 and the Institute of Particle Physics, Canada*
[3]*Ithaca College, Ithaca, New York 14850*
[4]*University of Kansas, Lawrence, Kansas 66045*
[5]*University of Minnesota, Minneapolis, Minnesota 55455*
[6]*State University of New York at Albany, Albany, New York 12222*
[7]*Ohio State University, Columbus, Ohio, 43210*
[8]*University of Oklahoma, Norman, Oklahoma 73019*
[9]*Purdue University, West Lafayette, Indiana 47907*
[10]*University of Rochester, Rochester, New York 14627*
[11]*Southern Methodist University, Dallas, Texas 75275*
[12]*Syracuse University, Syracuse, New York 13244*
[13]*Vanderbilt University, Nashville, Tennessee 37235*
[14]*Virginia Polytechnic Institute and State University, Blacksburg, Virginia, 24061*
[15]*California Institute of Technology, Pasadena, California 91125*
[16]*University of California, San Diego, La Jolla, California 92093*
[17]*University of California, Santa Barbara, California 93106*
[18]*University of Colorado, Boulder, Colorado 80309-0390*
[19]*Cornell University, Ithaca, New York 14853*
[20]*University of Florida, Gainesville, Florida 32611*
[21]*Harvard University, Cambridge, Massachusetts 02138*
[22]*University of Illinois, Champaign-Urbana, Illinois, 61801*

Abstract

Using 2.6×10^6 $B\bar{B}$ pairs accumulated with the CLEO II detector at the Cornell Electron Storage Ring, we update our measurement of $B^0 \to K^{*0}(892)\gamma$. We use a new background suppression technique in conjunction with a maximum likelihood fit and find $Br(B^0 \to K^{*0}\gamma) = (4.3^{+1.1}_{-1.0} \pm 0.6) \times 10^{-5}$.

I. INTRODUCTION

The radiative penguin decay $b \to s\gamma$ was first observed in the exclusive decay mode $B \to K^*(892)\gamma$ [1]. That discovery attracted a great deal of attention, since it was the first evidence for a penguin-loop induced Flavor-Changing-Neutral-Current process. These

---

*Permanent address: University of Hawaii at Manoa

Table I: Theoretical Predictions for the ratio $\Gamma(B \to K^*\gamma)/\Gamma(b \to s\gamma)$

Authors	$\Gamma(B \to K^*\gamma)/\Gamma(b \to s\gamma)$
Altomari (1988)	4.5 %
Deshpande *et al.* (1988)	7 %
Dominguez *et al.* (1988)	28 ± 11 %
Aliev *et al.* (1988)	39 %
Deshpande & Trampetic (1989)	$6 - 14$ %
Ali & Mannel (1991)	$18 - 28$ %
Faustov (1992)	6.5 %
Ali, Ohl & Mannel (1993)	$3.5 - 12.2$ %
El hassan & Riazuddin (1993)	$7 - 10$ %
Colangelo *et al.* (1993)	17 ± 5 %
O'Donnell & Tung (1993)	10 %
Ali & Greub (1993)	13 %
Ali, Braun & Simma (1993)	16 ± 5 %
Ball (1994)	20 ± 6 %
Bernard, Hsieh & Soni (1994)	$6.1 \pm 1.1 \pm 3.4$ %
Holdom & Sutherland (1994)	17 ± 4 %
Narison (1994)	16 ± 4 %
Bowler *et al.* (1994)	$9 \pm 3 \pm 1$ %
Ciuchini *et al.* (1994)	23 ± 9 %
Tang *et al.* (1995)	$10 - 12$ %

decays are of interest since they can interfere with the tree-diagram amplitude to produce direct CP asymmetry. In the Standard Model, the only source of CP violation is attributed to the phases of the CKM matrix. In future B-factories we will be able to test this explanation of the origin of CP violation via direct CP asymmetry measurements.

The total $b \to s\gamma$ rate has also been measured recently by CLEO [2]. The rate is in good agreement with theoretical predictions [3], providing stringent constraints on physics beyond the Standard Model [4]. In contrast, calculations of rates for exclusive channels, such as $B \to K^*\gamma$, have been marred by uncertainty in $B \to K^*$ form factors. Various models predict the ratio, $r = \Gamma(B \to K^*\gamma)/\Gamma(b \to s\gamma)$ to be in the range $4\% < r < 40\%$, as shown in Table I [5]. Precise measurement of this ratio can help to establish credibility in the non-perturbative QCD regime for some of these theoretical models. This in turn may help to decrease model dependence when extracting CKM matrix elements from experimental data.

The data used in this analysis were taken with the CLEO-II detector at the Cornell Electron Storage Ring (CESR). They consist of 2.40 fb^{-1} of integrated luminosity on the $\Upsilon(4S)$ resonance (2.57×10^6 $B\bar{B}$ events) and 1.14 fb^{-1} at a center-of-mass energy 60 MeV below the resonance.

The CLEO-II detector is a general purpose solenoidal detector designed to detect charged and neutral particles with high efficiency and good resolution [6]. Charged particles are tracked with three concentric cylindrical wire chambers operating in a 1.5 T magnetic field. The outer chamber (main drift chamber) provides charge particle identification via specific ionization (dE/dx) measurement. Further particle identification is achieved with a scintillation layer, Time of Flight (ToF), just outside the main drift chamber. An electromagnetic calorimeter is used for photon reconstruction. The calorimeter comprises 7800 CsI crystals positioned inside the magnet and has an excellent resolution of $\sigma_E/E = 2\%$ for $E \approx 2$ GeV in the central portion of the detector.

II. EVENT SELECTION

The dominant backgrounds for this study arise from continuum $q\bar{q}$ production. We divide the continuum into two separate categories based on the origin of the high energy photon: from decay of π^0 or η in $q\bar{q}$ events ($Q\bar{Q}$) and from initial state radiation (ISR). To separate these backgrounds from the $B^0 \to K^{*0}\gamma$ signal we apply a series of cuts based on Monte Carlo studies.

The photon candidates are formed from clusters in the electromagnetic calorimeter. These photons must have an energy in the range $2.0 < E_\gamma < 3.0$ GeV, have a polar angle θ_γ (relative to the beam axis) satisfying $|\cos\theta_\gamma| < 0.71$, not be matched to a charged track, and have a shower shape consistent with a single photon. Photons are rejected if they form π^0's (η's) when combined with another photon of energy greater than 30 (200) MeV.

The candidate K^{*0}'s are formed from two charged tracks, where one track is assigned to be a K, the other a π. Each track must pass standard track quality cuts and must have a value of ToF and/or dE/dx less than 2.5 standard deviations from its particle hypothesis. The K^{*0} formed from this pair of tracks is required to have a mass within $\pm 3\Gamma_{K^{*0}}$ ($746 < M_{K\pi} < 1046$ MeV).

By combining the two tracks from the K^{*0} with the photon, we form a B candidate. Wide cuts on the energy and mass of the B are applied to maximize the signal efficiency and to provide a signal-free region for background estimation. When calculating the B's energy we avoid the $K\pi$ or πK particle identification ambiguity by assigning both tracks to have a π mass. This causes $\Delta E = E_{\pi\pi\gamma} - E_{beam}$ to be centered at –77 MeV. We require that the B satisfy $-350 < \Delta E < 200$ MeV. Since the energy of the B must be equal to the beam energy, the reconstructed mass of the B is given by

$$M_B = \sqrt{E_{beam}^2 - (\vec{P}_\gamma + \vec{P}_{K^{*0}})^2}.$$

Using the well measured CESR beam energy results in a mass resolution of $\sigma(M_B) = 2.7$ MeV. This is an order of magnitude improvement over using the measured energies of the daughters. For this analysis we require $5.2 < M_B < 5.3$ GeV.

Once the candidates have been chosen, the event must pass a series of event shape cuts. Both B mesons in a $B\bar{B}$ event are produced approximately at rest in the lab frame. The decays of the two B mesons are uncorrelated, therefore producing a spherical event shape. In contrast, $Q\bar{Q}$ events tend to have a two-jet topology. ISR events lie between the two extremes. To exploit these differences cuts are placed on the shape variables R_2, the second Fox-Wolfram moment [7], and $\cos\theta_{thrust}$, where θ_{thrust} is the angle between the photon's direction and the thrust axis of the rest of the event excluding the K, π, and γ candidates.

We require $R_2 < 0.7$ and $|\cos\theta_{thrust}| < 0.65$. Additional shape variables used for the maximum likelihood fit are discussed below.

All combined, these cuts have a signal efficiency of 24.8%. Factoring in the branching fraction $Br(K^{*0} \to K^+\pi^-) = 66.7\%$, this gives an overall efficiency of $(16.5 \pm 1.3)\%$ where the error is systematic and will be discussed in section VI. After all cuts, 137 events remain.

III. ADDITIONAL EVENT SHAPE ANALYSIS

To further exploit the shape differences between $B^0 \to K^{*0}\gamma$ signal and the two backgrounds we use a Fisher discriminant. A Fisher discriminant [8,9] combines several variables which individually may only marginally separate signal and background to get one variable which has good signal to background separation. The Fisher discriminant is a linear combination of the input variables

$$\mathcal{F} = \sum_{i=1}^{N_v} \alpha_i x_i$$

where α_i is the coefficient for the ith input variable, x_i. The coefficients are calculated to maximize the separation between signal and background and are derived from

$$\alpha_i = \sum_{j=1}^{N_v} (U^b_{ij} + U^s_{ij})^{-1} \times (\mu^s_j - \mu^b_j),$$

where U^b_{ij} and U^s_{ij} are the covariance matrices in the input variables for background and signal events, and μ^b_j, μ^s_j are the mean values of the input variables.

Twelve shape variables are used in the Fisher discriminant: nine momentum cones, $\cos\theta_B$, and one eigenvalue of the momentum tensor. The nine momentum cones are about an axis along the photon candidate's direction, and each cone covers a 20° polar angle, with the nine cones filling the entire 180° range. All momenta from well measured charged tracks and unmatched showers (excluding the B candidate's daughters) which lie within a cone are summed together to form the output for the cone. We define θ_B as the angle between the candidate B's flight direction and the electron/positron beam axis. Signal has a $\sin^2\theta_B$ distribution while background is flat. The final input to the Fisher discriminant is the largest eigenvalue of the momentum tensor where the tensor is computed from all the well measured charged tracks and unmatched showers in the event, excluding the candidate photon. Empirical testing determined that these twelve variables gave the best signal to background separation. To calculate the Fisher coefficients, α_i, we use Monte Carlo samples of $B^0 \to K^{*0}\gamma$ signal and $Q\bar{Q}$ background. The output from the Fisher discriminant for Monte Carlo samples of signal, $Q\bar{Q}$, and ISR is shown in Figure 1.

When we place a cut on the Fisher discriminant such that the overall efficiency of the analysis is the same as the previous CLEO $B^0 \to K^{*0}\gamma$ analysis [1], ISR background is reduced by 20% compared to the previous analysis and $Q\bar{Q}$ background is reduced by 55%. Since the signal to background ratio is already fairly large for this analysis, we do not place a cut on the Fisher discriminant. Instead we use the Fisher discriminant output in a maximum likelihood fit.

IV. MAXIMUM LIKELIHOOD FIT

We are interested in distinguishing between three event types: $B^0 \to K^{*0}\gamma$ signal, $Q\bar{Q}$, and ISR. To accomplish this we form a likelihood function using five variables to characterize an event

$$\mathcal{L} = \prod_{event=1}^{137} \Big\{ f_{signal} P_{signal}(\mathcal{F}, M_B, M_{K^{*0}}, \Delta E, \cos\theta_{decay}) \\ + (1 - f_{signal}) \cdot [f_{Q\bar{Q}} P_{Q\bar{Q}}(...) \ + \ (1 - f_{Q\bar{Q}}) P_{ISR}(...)] \Big\}_{event}$$

where f_{signal} is the fraction of signal events in the sample, $f_{Q\bar{Q}}$ is the fraction of $Q\bar{Q}$ events over the total number of background events and P_{signal}, $P_{Q\bar{Q}}$, and P_{ISR} are the probability distribution functions for signal, $Q\bar{Q}$, and ISR respectively. Maximizing the likelihood function by varying f_{signal} and $f_{Q\bar{Q}}$ will find the values of these two fractions that best match the 137 events that passed all the selection criteria. The fraction of ISR is fixed by the overall normalization.

The values of the Fisher discriminant output ($\mathcal{F}$), M_B, $M_{K^{*0}}$, and ΔE, are calculated as described in the previous two sections. The decay angle, θ_{decay}, is the angle between the K^{*0}'s direction in the lab frame and the K^{*0}'s fastest daughter's direction in the K^{*0}'s rest frame. We find the rest frame assuming the two daughters are both π's rather than a K and a π. This makes $\cos\theta_{decay}$ invariant under the interchange of K and π identities and does not significantly change the $\sin^2\theta_{decay}$ distribution of the signal.

If one event had multiple B candidates (usually due to the assignment of the K and π masses between the two tracks) the candidate with the smallest $|E_K + E_\pi + E_\gamma - E_{beam}|$ value is chosen. This happens in less than 5% of the events.

To determine the functional form of each of the three probability distribution functions (pdf's), we assume that the five likelihood variables are uncorrelated. Therefore each pdf is just the product of the probability for each of the likelihood variables. The shape of each likelihood variable for each of the three possible event hypotheses is found by fitting the corresponding distribution obtained from Monte Carlo events. The parameterized shapes are normalized and used to calculate the probabilities P_{signal}, $P_{Q\bar{Q}}$, and P_{ISR}.

The number of signal events obtained from the fit is

$$\begin{aligned} N_{signal} &= N_{events} f_{signal} \\ &= (137 \pm 12) \times (0.134^{+0.034}_{-0.031}) \\ &= 18.4^{+4.9}_{-4.5}. \end{aligned}$$

Band projections of the data and fit functions onto the five inputs are shown in Figures 2 and 3. Each band projection is obtained by placing tighter cuts on the four input variables not plotted in the projection and then rescaling the fit function area based on the number of events of that type which would pass the tighter cuts. All band projections show reasonably good agreement with the data.

Table II: Summary of $B^0 \to K^{*0}\gamma(K^{*0} \to K^+\pi^-)$ Results

	present analysis	previous analysis [1]
Luminosity	2.4 fb^{-1}	1.4 fb^{-1}
Efficiency	$(16.5 \pm 1.3)\%$	$(11.9 \pm 1.8)\%$
Total Events	137	49
Signal Events	$18.4^{+4.9}_{-4.5}$	6.6 ± 2.8
Branching Ratio	$(4.3^{+1.1}_{-1.0} \pm 0.6) \times 10^{-5}$	$(4.0 \pm 1.7 \pm 0.8) \times 10^{-5}$

V. RESULTS

The result of the maximum likelihood fit is shown in Table II. From the likelihood fit, the net yield of $B^0 \to K^{*0}\gamma$ events is $18.4^{+4.9}_{-4.5}$. The data sample contains 2.57×10^6 $B\bar{B}$ decays, which we assume to be half charged and half neutral. Combining these with the signal efficiency we obtain a branching ratio for $B^0 \to K^{*0}\gamma$ of $(4.3^{+1.1}_{-1.0} \pm 0.6) \times 10^{-5}$, where the first error on the branching ratio is statistical and the second is an estimate of the systematic uncertainty from the efficiency and the maximum likelihood fit. Table II also shows a comparison between this analysis and the previous CLEO analysis. The results are in good agreement.

There are three main differences between the two analyses: amount of luminosity used, the method of continuum suppression, and event counting versus maximum likelihood fitting. The previous analysis cut on four specific shape variables, each of which separated the signal events from $Q\bar{Q}$ and/or ISR. In this analysis twelve correlated shape variables are combined using a Fisher discriminant. Rather than cutting on the output of the Fisher discriminant, this variable is used in the maximum likelihood fit, and hence we gain in signal efficiency.

VI. SYSTEMATICS

The results of the study of systematic uncertainties from the likelihood fit are shown in Table III. The values are obtained by varying the fit parameters for each probability distribution function and measuring the percentage change in f_{signal}. The $Q\bar{Q}$ and ISR pdf shapes are varied by the amount allowed from a fit to background data (below $\Upsilon(4S)$ resonance and on resonance excluding the signal region). Most of the signal pdf shape variations are determined by using the known differences between Monte Carlo and data or varying the E_γ resolution in the Monte Carlo. The largest contribution to the systematic uncertainty is from the signal Fisher output shape. A Gaussian is used to parameterize the Fisher output shape for $Q\bar{Q}$, ISR and signal. The average of the variations on the $Q\bar{Q}$ and ISR means and standard deviations is used for the variations of the signal parameters.

The systematic uncertainty on the signal efficiency is 7.6%. The two largest contributions to this uncertainty are from the $\cos\theta_{thrust}$ cut and the photon candidate's π^0 and η suppression cut, both of which have a 3% systematic uncertainty. The quadratic sum of the

Table III: Summary of Likelihood Fit Systematic Uncertainties

$\mathcal{F}$	M_B	$M_{K^{*0}}$	ΔE	$\cos\theta_{decay}$	Total
$\pm 10.8\%$	$\pm 5.2\%$	$\pm 2.8\%$	$\pm 2.1\%$	$\pm < 1\%$	$\pm 12.4\%$

likelihood fit and signal efficiency systematic uncertainties is well below the statistical error on the measurement.

VII. CONCLUSION

We have remeasured the branching ratio for the exclusive decay channel $B^0 \to K^{*0}\gamma$:

$$Br(B^0 \to K^{*0}\gamma) = (4.3^{+1.1}_{-1.0} \pm 0.6) \times 10^{-5},$$

which is consistent with the previous CLEO measurement [1]. Improvement in the statistical uncertainty is at the level expected from the relative size of data samples, while the systematic uncertainty was reduced with better understanding of reconstruction efficiency.

Using the earlier measurement of the inclusive rate [2], we determine the ratio,

$$r = \Gamma(B \to K^*\gamma)/\Gamma(b \to s\gamma) = 0.19 \pm 0.07 \pm 0.04.$$

This result tends to disfavor some of the smaller predictions in Table I, as well as the high value of Aliev, *et al.* [5], although none is decisively ruled out.

New analyses for $B^+ \to K^{*+}\gamma$ modes as well as $B \to (\rho,\omega)\gamma$ using the same techniques as this analysis are underway.

ACKNOWLEDGEMENTS

We gratefully acknowledge the effort of the CESR staff in providing us with excellent luminosity and running conditions. This work was supported by the National Science Foundation, the U.S. Department of Energy, the Heisenberg Foundation, the Alexander von Humboldt Stiftung, the Natural Sciences and Engineering Research Council of Canada, and the A.P. Sloan Foundation.

REFERENCES

[1] R. Ammar *et al.* (CLEO Collaboration), Phys. Rev. Lett. **71**, 674 (1993).

[2] M.S. Alam *et al.* (CLEO Collaboration), Phys. Rev. Lett. **74**, 2885 (1995).

[3] S. Bertolini, F. Borzumati, and A. Masiero, Phys. Rev. Lett. **59**, 180 (1987); N.G. Deshpande *et al.*, Phys. Rev. Lett. **59**, 183 (1987); B. Grinstein, R. Springer, and M.B. Wise, Phys. Lett. B **202**, 138 (1988); R. Grigjanis *et al.*, Phys. Lett. B **213**, 355 (1988); A. Ali and C. Greub, Z. Phys. C **49**, 431 (1991); M. Ciuchini *et al.*, Phys. Lett. B **316**, 127 (1991); M. Misiak, Phys. Lett. B **321**, 113 (1994); G. Cella *et al.*, Phys. Lett. B **325**, 227 (1994).

[4] For example see J. Hewett, SLAC-PUB-6521 (1994) and references therein.

[5] T. Altomari, Phys. Rev. D **37**, 677 (1988); C.A. Dominguez *et al.*, Phys. Lett. B **214**, 459 (1988); N.G. Deshpande *et al.*, Z. Phys. C **40**, 369 (1988); T.M. Aliev *et al.*, Phys. Lett. B **237**, 569 (1988); P.J.O'Donnell and H.K.K. Tung, Phys. Rev. D **44**, 741 (1991), *ibid* **48**, 2145 (1993); A. Ali and C. Greub, Phys. Lett. B **259**, 182 (1991), Z. Phys. C **60**, 433 (1993); A. Ali and T. Mannel, Phys. Lett. B **264**, 447 (1991); R.N. Faustov, Mod. Phys. Lett. A **7**, 2111 (1992); A. Ali, T. Ohl, and T. Mannel, Phys. Lett. B **298**, 195 (1993); El hassan El aaoud, Riazuddin, Phys. Rev. D **47**, 1026 (1993); P. Colangelo *et al.*, Phys. Lett. B **317**, 183 (1993); A. Ali, V.M. Braun, and H. Simma, Z. Phys. C **63**, 437 (1994); P. Ball, TUM-T31-43-93; C. Bernard, P. Hsieh, and A. Soni, Phys. Rev. Lett, **72**, 1402 (1994); S. Narison, Phys. Lett. B **327**, 354 (1994); B. Holdom and M. Sutherland Phys. Rev. D **49**, 2356 (1994); K.C. Bowler *et al.*, Edinburgh-94-544; M. Ciuchini *et al.*, Phys. Lett. B **334**, 137 (1994); J. Tang *et al.*, Phys. Rev. D **51**, 3501 (1995);

[6] Y. Kubota *et al.* (CLEO Collaboration), Nucl. Instrum. Methods Phys. Res. Sect. A **320**, 66 (1992).

[7] G. Fox and S. Wolfram, Phys. Rev. Lett. **41**, 158 (1978).

[8] R. A. Fisher, "The Use of Multiple Measurements in Taxonomic Problems", *Annals of Eugenics*, **7**, 179 (1936).

[9] M.G. Kendall and A. Stuart, *The Advanced Theory of Statistics* , Vol. III, 2nd Ed., Hafner Publishing, NY, (1968).

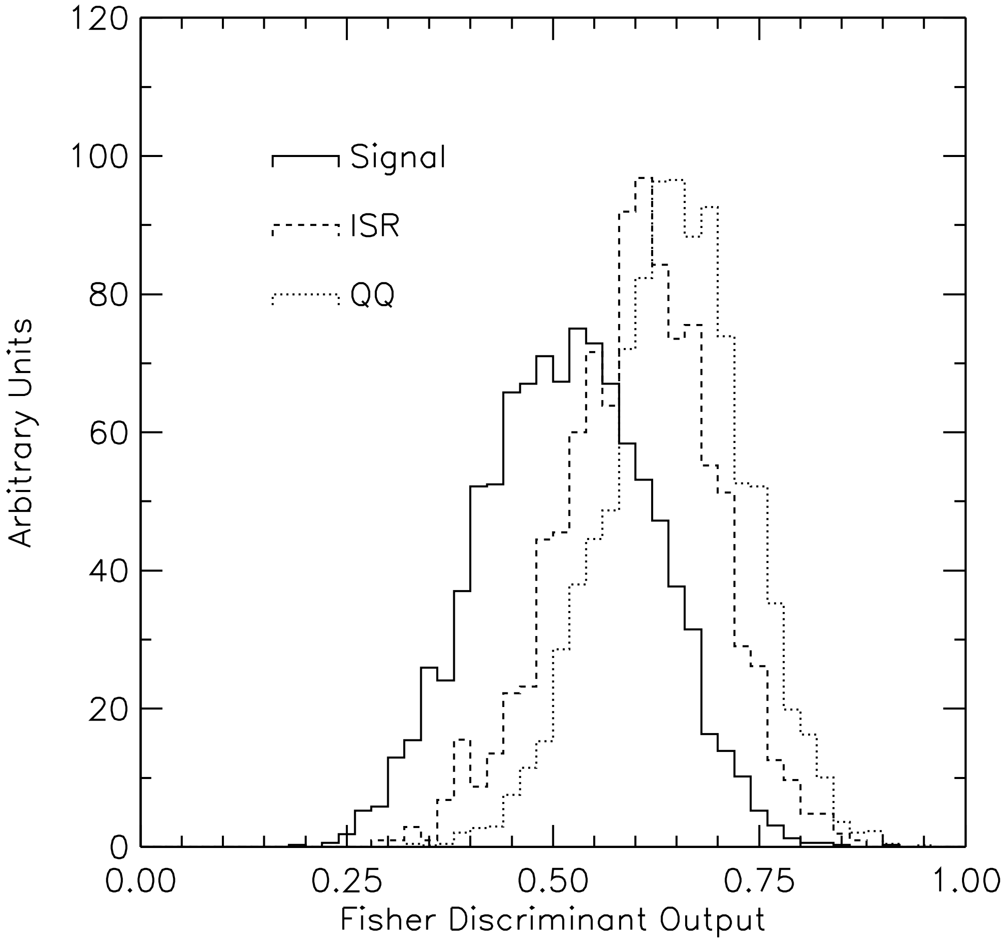

FIG. 1. Fisher discriminant output for Monte Carlo samples of $B^0 \to K^{*0}\gamma$ signal (solid line), ISR (dashed), and $Q\bar{Q}$ (dotted).

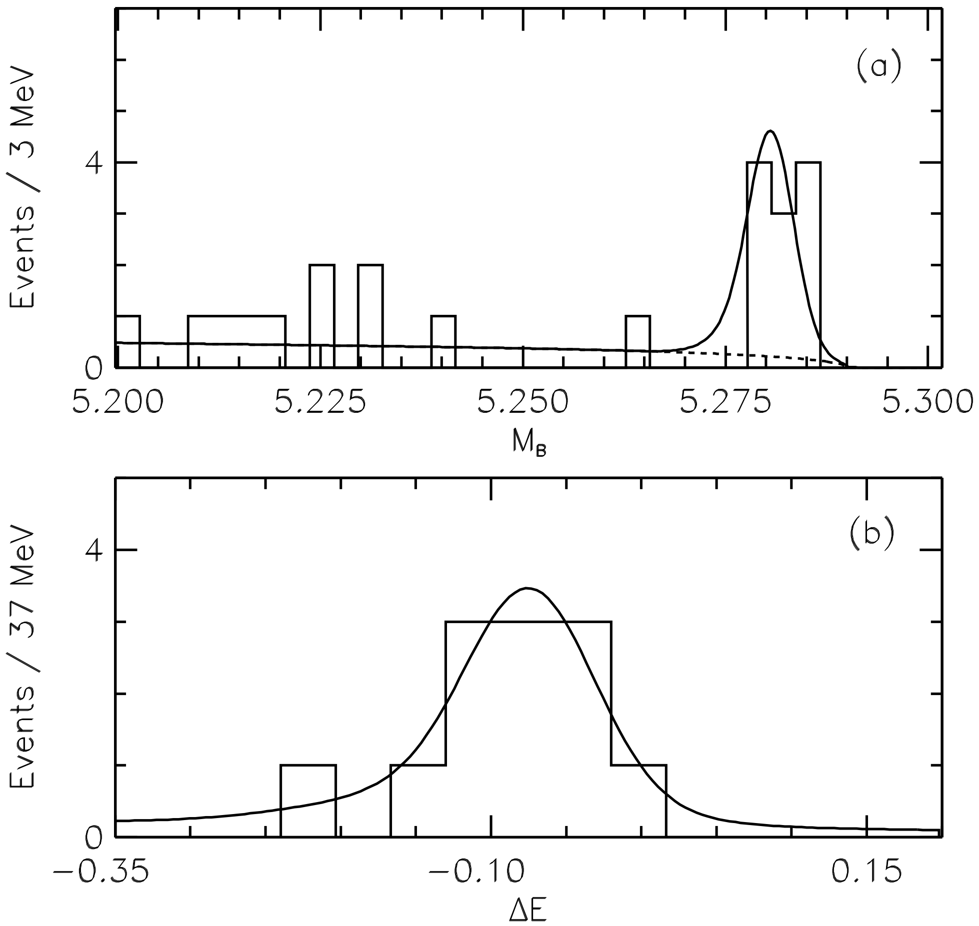

FIG. 2. Band projections of the data and maximum likelihood fit onto the maximum likelihood variables: (a) M_B and (b) ΔE. Each band projection is obtained by placing tighter cuts on the four other input variables and then rescaling the fit function area based on the efficiency of the additional cuts. The dashed line in (a) shows the amount of background under the signal peak. The curves are not fits to the histograms shown.

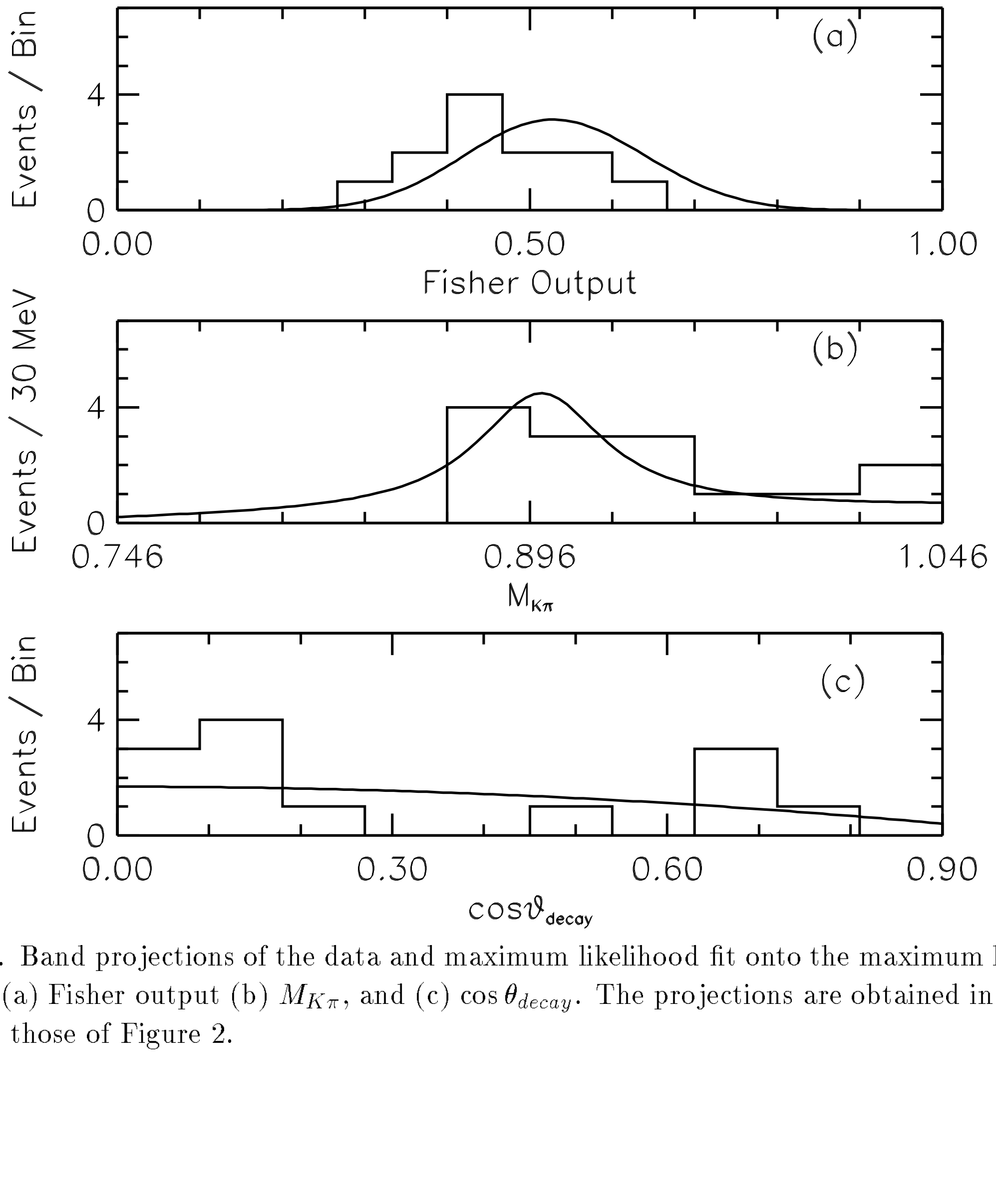

FIG. 3. Band projections of the data and maximum likelihood fit onto the maximum likelihood variables: (a) Fisher output (b) $M_{K\pi}$, and (c) $\cos\theta_{decay}$. The projections are obtained in the same manner as those of Figure 2.